Ultralight Multiwalled Carbon Nanotube Aerogel

Jianhua Zou,[†] Jianhua Liu,[†] Ajay Singh Karakoti,[§] Amit Kumar,[§] Daeha Joung,[¶] Qiang Li,[†] Saiful I. Khondaker,[¶] Sudipta Seal,[§,⊥] and Lei Zhai[†,‡,*]

[†]NanoScience Technology Center, [‡]Department of Chemistry, [§]Advanced Materials Processing and Analysis Center, [⊥]Department of Mechanical, Materials and Aerospace Engineering, and [¶]Department of Physics, University of Central Florida, Orlando, Florida 32826, United States

ABSTRACT Ultralight multiwalled carbon nanotube (MWCNT) aerogel is fabricated from a wet gel of well-dispersed pristine MWCNTs. On the basis of a theoretical prediction that increasing interaction potential between CNTs lowers their critical concentration to form an infinite percolation network, poly(3-(trimethoxysilyl) propyl methacrylate) (PTMSPMA) is used to disperse and functionalize MWCNTs where the subsequent hydrolysis and condensation of PTMSPMA introduces strong and permanent chemical bonding between MWCNTs. The interaction is both experimentally and theoretically proven to facilitate the formation of a MWCNT percolation network, which leads to the gelation of MWCNT dispersion at ultralow MWCNT concentration. After removing the liquid component from the MWCNT wet gel, the lightest ever free-standing MWCNT aerogel monolith with a density of 4 mg/cm^3 is obtained. The MWCNT aerogel has an ordered macroporous honeycomb structure with straight and parallel voids in 50−150 μm separated by less than 100 nm thick walls. The entangled MWCNTs generate mesoporous structures on the honeycomb walls, creating aerogels with a surface area of 580 m^2/g which is much higher than that of pristine MWCNTs (241 m^2/g). Despite the ultralow density, the MWCNT aerogels have an excellent compression recoverable property as demonstrated by the compression test. The aerogels have an electrical conductivity of 3.2×10^{-2} S · cm^{-1} that can be further increased to 0.67 S · cm^{-1} by a high-current pulse method without degrading their structures. The excellent compression recoverable property, hierarchically porous structure with large surface area, and high conductivity grant the MWCNT aerogels exceptional pressure and chemical vapor sensing capabilities.

KEYWORDS: carbon nanotube aerogel · honeycomb · hierarchically porous · pressure sensor · gas sensor

Assembling carbon nanotubes (CNTs) into bulk materials with desired structures and properties holds the key to realize their extensive applications. For example, CNT sheet represents one of the most attractive CNT bulk materials[1−3] and is considered an alternative to indium tin oxide (ITO) for transparent electrode materials.[4−6] The fibers spun from CNTs were demonstrated to combine both high strength and high stiffness derived from individual CNTs.[7,8] The vertically aligned CNT forest has found important applications in field emission displays[9] and flexible energy storage devices.[10,11] Assembling CNTs into aerogels creates a new CNT bulk material that integrates the intriguing properties of CNTs[12−17] with the unique structures and related properties of aerogels. Aerogels are low density, highly porous materials with large surface area,[18−23] offering a wide range of applications as thermal[20] and acoustic[21] insulating materials, catalyst support,[22] and electrodes for supercapacitors.[23] Although aerogels have been fabricated from silica, metal oxides, polymers, and carbon-based materials,[19] fabricating CNT aerogels is still challenging with only a few successful examples.[2,8,24] During the process of producing CNT sheets[2] and drawing nanotube fibers,[8] aerogels were produced as intermediate phases, which were not free-standing monoliths and eventually collapsed into dense structures. Free-standing CNT aerogels were fabricated from a CNT wet gel formed by sodium dodecylbenzene sulfonate (NaDDBS) dispersed CNTs.[24] Owing to the low mechanical strength of the obtained CNT aerogels, poly(vinyl alcohol) was incorporated for the reinforcement, which decreased the conductivity and increased the density of the aerogels. Most recently, a sponge-like CNT material was fabricated by a CVD process. The obtained CNT sponges have a density of 5.8−25.5 mg/cm^3 and surface area of 300−400 m^2/g, and have demonstrated interesting oil spill cleanup properties.[25]

In this paper, we report a solution-based approach to fabricating an ultralight free-standing MWCNT aerogel monolith. This approach is based on the theoretical prediction that increasing interaction potentials between CNTs decreases their critical concentration to form an infinite percolation network,[26,27] which is responsible for the gelation of a fluid system according to the percolation model.[28,29] Therefore, introducing intense interactions between CNTs represents a potential solution to induce the

*Address correspondence to lzhai@mail.ucf.edu.

Received for review September 1, 2010 and accepted November 15, 2010.

Published online November 22, 2010. 10.1021/nn102246a

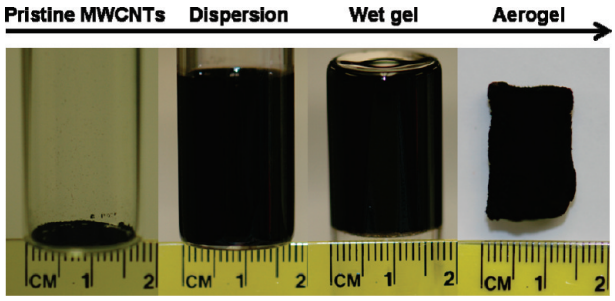

Figure 1. Fabrication procedure of MWCNT aerogel illustrated by pictures of each fabrication step.

gelation of a MWCNT dispersion at ultralow CNT concentration, which can be further processed to fabricate ultralight CNT aerogels. In our study, we functionalized MWCNTs with poly(3-(trimethoxysilyl) propyl methacrylate) (PTMSPMA).[30−32] PTMSPMA is a reactive polymer with two functions: (1) dispersing and stabilizing MWCNTs as individual tubes in solutions and (2) introducing permanent and intense chemical bonding between MWCNTs by the formation of cross-linked polysilsesquioxane through the hydrolysis and condensation of PTMSPMA. The intense chemical bonding interactions between MWCNTs decrease their percolation threshold and lead to the formation of MWCNT wet gels with low MWCNT concentration. The removal of the solvent from wet gels generates the lightest free-standing MWCNT aerogels with a density of 4 mg/cm^3. The MWCNT aerogels have a honeycomb structure, hierarchical porosity with a surface area of 580 m^2/g, excellent compression recoverable property, and a high electrical conductivity, making them interesting pressure and chemical vapor sensing materials.

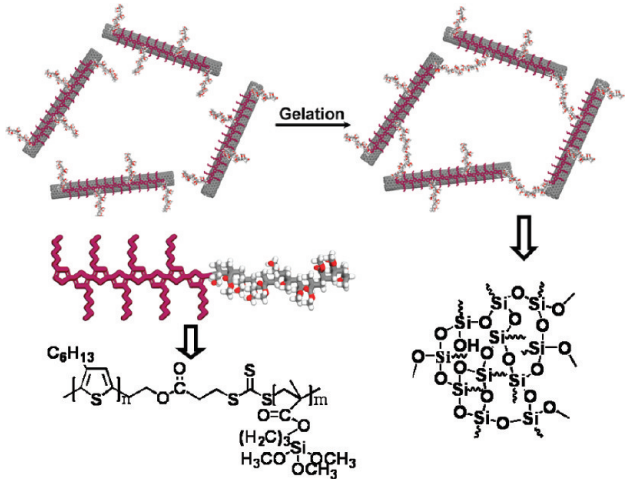

Scheme 1. Schematic illustration of gelation process of P3HT-*b*-PTMSPMA dispersed MWCNTs. Before gelation, P3HT blocks bond to the MWCNT surface through π−π interaction; PTMSPMA blocks locate at the outer surface of MWCNT. After gelation, MWCNTs interact with each other through chemical bonding formed by PTMSPMA blocks.

TABLE 1. Characteristics of Three P3HT-*b*-PTMSPMAs, the CGC of the CNT Wet Gel, and the Density and Conductivity of Dispersed MWCNT Aerogels

	P3HT-*b*-PTMSPMA 1	P3HT-*b*-PTMSPMA 2	P3HT-*b*-PTMSPMA 3
M_n	18700	21900	27600
$M_{n\ PTMSPMA}$	9600	13000	18300
CGC[a]	1.2/0.053%	0.3/0.014%	0.3/0.014%
density[b]	11.6	4.0	5.8
conductivity[c]	0.26	3.2×10^{-2}	7.9×10^{-3}

[a]The numbers represent the mass volume CGC in unit of mg/mL and volume fraction CGC, respectively. [b]The density (mg/cm^3) of the MWCNT aerogel fabricated from different P3HT-*b*-PTMSPMAs at the CGC of MWCNTs. [c]The conductivity (S · cm^{-1}) of MWCNT aerogel fabricated from different P3HT-*b*-PTMSPMAs at the CGC of MWCNTs.

RESULTS AND DISCUSSION

The Fabrication of MWCNT Aerogels. Figure 1 illustrates the fabrication procedure of MWCNT aerogels from pristine MWCNTs by presenting the pictures taken at each step of the MWCNT aerogel fabrication process. Pristine MWCNTs were dispersed as individual tubes in chloroform by poly(3-hexylthiophene)-*b*-PTMSPMA (P3HT-*b*-PTMSPMA) *via* a sonication of 13 min (Supporting Information, Figure S1). According to our previous investigations,[30−32] the dispersed MWCNTs have PTMSPMA on their surfaces through the binding of P3HT block to MWCNT surface *via* π−π interactions (Scheme 1). As compared to other methods to functionalize CNTs with PTMSPMA, such as encapsulating CNTs by vesicles formed by PTMSPMA-PEG copolymers[33] and MWCNT surface-initiated polymerization,[34] our approach provides a nondestructive method to uniformly anchor PTMSPMA on MWCNT surfaces with controllable density. The MWCNT dispersion set into a wet gel in several minutes to several hours, which was inversely proportional to the concentration of MWCNT (Supporting Information, Table S1). The obtained MWCNT wet gel was aged for 12 h at room temperature and then applied to a solvent-exchange process with methanol to remove chloroform. Subsequently, an ammonia aqueous solution was added to cross-link the MWCNT wet gel for 12 h by the hydrolysis and condensation of PTMSPMA. Shrinkage of the wet gel was observed during this process indicating the successful cross-linking. After removing methanol and ammonia by exchanging with water, the wet gel was freeze-dried to obtain the MWCNT aerogels.

Mechanism of MWCNT Wet Gel Formation. Three P3HT-*b*-PTMSPMAs with different PTMSPMA molecular weight ($M_{n\ PTMSPMA}$) but same P3HT molecular weight (Table 1) were applied to disperse MWCNTs at a ratio of 1 mg MWCNTs to 8.5 × 10^{-5} mmol P3HT-*b*-PTMSPMA to achieve the same PTMSPMA polymer chain density on a MWCNT surface (Supporting Information). Such process assures the same PTMSPMA polymer chain density on MWCNT surfaces for the subsequent investigation

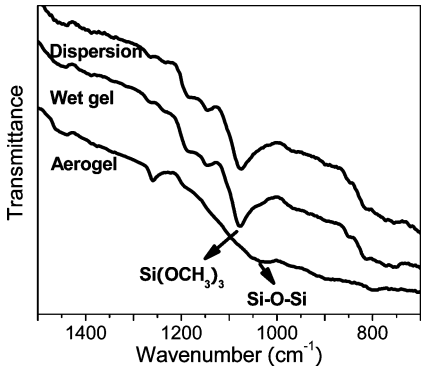

Figure 2. FTIR spectra of the MWCNT dispersion, wet gel, and aerogel.

of the impact of $M_{n\ PTMSPMA}$ on the critical gelation concentration (CGC), which is defined as the lowest MWCNT concentration that forms a wet gel (Table 1). The CNT wet gels have been produced by several groups and their formation is ascribed to the interactions among CNTs.[35−38] For example, sodium dodecylbenzenesulfonate (NaDDBS)-dispersed CNTs gelate at a concentration of 5 mg/mL, and the gelation is believed to be induced by the CNT attraction arising from osmotic pressure of NaDDBS-formed micelles.[35] CNTs functionalized by ferrocene-grafted poly(*p*-phenyleneethynylene) (PPE) show a CGC of 4 mg/mL in chloroform due to the interaction among CNTs through ferrocene groups.[36] CNTs (>1 wt %) form a wet gel in ionic liquid, where the local molecular ordering of the ionic liquid mediates the physical cross-linking of the CNTs.[37] Oxidized CNTs in aqueous solutions form gels when the CNT concentration is above 0.3 wt % due to the interactions between CNTs through hydrogen bonds.[38] In these studies, physical interaction between CNTs is the key for the gelation process in different gel systems. Since the interaction potential determines the CNT threshold of percolation network which leads to the wet gel formation, it is not surprising to observe comparable CGCs (several milligrams of CNT per milliliter solvent) in all these CNTs wet gels. In our study, the lowest CGC of MWCNTs was characterized to be 0.3 mg/mL (Table 1), which is 10 times less than the literature-recorded CGCs. Such a low CGC indicates the presence of strong interactions between MWCNTs since the percolation threshold is reversibly proportional to the interaction potential between CNTs. We believe that the intense interactions originate from the chemical bonding formed by the cross-link of PTMSPMA to polysilsesquioxane. As illustrated in Scheme 1, the cross-link of the PTMSPMAs attached on individual MWCNT introduces chemical bonding interactions between MWCNTs. The proposed chemical bonding interaction induced gelation mechanism was proved by the FTIR studies of MWCNT dispersion, wet-gels, and aerogels. As shown in Figure 2, the spectrum of a freshly prepared P3HT-*b*-PTMSPMA/MWCNT dispersion shows the stretching vibration band of $Si(OCH_3)_3$ of the PTMSPMA at 1077 cm^{-1}. The MWCNT wet gel exhibits an identical spectrum except that a small shoulder at 1030 cm^{-1} assigned to Si−O−Si of polysilsesquioxane is observed,[39] suggesting that PTMSPMA blocks partially cross-link during the gelation process. The $Si(OCH_3)_3$ peak at 1077 cm^{-1} decreases significantly and a broad peak of Si−O−Si appears at 1030 cm^{-1} for the MWCNT aerogels, suggesting that most PTMSPMA blocks have cross-linked. The PTMSPMA cross-linking induced gelation mechanism was also proved by several control experiments. First, MWCNTs dispersed by P3HT homopolymer do not form wet gels, indicating the critical role of PTMSPMA in the wet gel formation. Second, the MWCNT wet gel cannot be redispersed by various approaches including sonication, agitation, dilution, and heating, showing that MWCNTs are cross-linked through permanent chemical bonding interactions. Third, when P3HT-*b*-PTMSPMA itself is sonicated in chloroform for 13 min and then kept at room temperature for 12 h, the polymer becomes insoluble, which is analyzed to be due to the hydrolysis and condensation of PTMSPMA block. Forth, in contrast to the formation of physical-interaction mediated wet gel, which is usually triggered by cooling the sol precursor down to a certain temperature,[40] the gelation of our MWCNT dispersion is facilitated at high temperature, which promotes the cross-linking reaction of PTMSPMA (Supporting Information, Table S1).

To quantitatively verify the chemical bonding interaction induced gelation mechanism, we investigated the CGC of MWCNTs dispersed by P3HT-*b*-PTMSPMAs with different $M_{n\ PTMSPMA}$. When the density of the PTMSPMA chain on MWCNT is kept constant *via* control of the MWCNT/polymer ratio, the intensity of the interaction can be manipulated by $M_{n\ PTMSPMA}$, which determines the number of chemical bondings between MWCNTs. As shown in Table 1, the CGC of MWCNTs decreases dramatically from 1.2 to 0.3 mg/mL when $M_{n\ PTMSPMA}$ increases from 9600 to 13000. However, the CGC remains a constant of 0.3 mg/mL when $M_{n\ PTMSPMA}$ further increases to 18300. To quantitatively account for these results, eq 1,[41] derived from pair-connectedness theory which describes the distribution of physical clusters of particles,[42−44] was applied to establish the connection between the percolation threshold and interaction potentials between MWCNTs.

$$\varphi_p = 4Ld^2/\left[2L^2d\int_{\gamma^c}^{\pi/2}\exp\left(\frac{\beta w_\perp}{\sin\gamma}\right)\sin(\gamma)\,d\gamma + 4d^2\int_0^L \exp\left(\frac{\beta w_\perp}{d}z\right)dz\right] \quad (1)$$

In eq 1, φ_p represents the volume-fraction-based percolation threshold. In our calculation, we considered the CGC as φ_p since the percolation threshold has

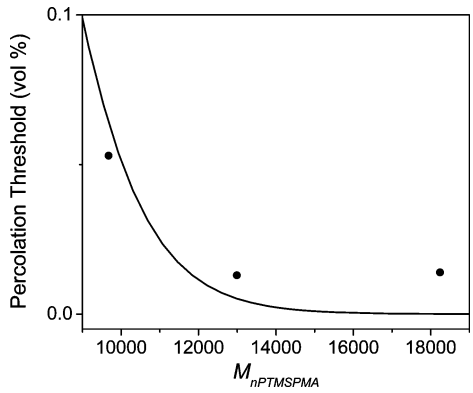

Figure 3. Percolation threshold of MWCNTs as a function of molecular weight of PTMSPMA ($M_{n\,PTMSPMA}$) with solid dots (●) and solid line (—) representing the experimental result and theoretical calculation, respectively.

been proved to coincide with the CGC.[26,45] Volume fraction was deduced from mass volume concentration (mg/mL) by taking the purity (95 wt %) and density (2.1 g/cm^3 for small cavity MWCNTs)[46] of MWCNTs into account (Table 1). L and d represented the length (4.85 μm) and diameter (21.6 nm) of MWCNTs, which are assumed to be monodispersed;[47] γ was the angle between two interacted MWCNTs with γ^c given by $\sin \gamma^c = d/L$. $\beta = 1/(kT)$ with k denoting Boltzmann's constant and T representing the temperature; $w_\perp$ is the interaction potential between two perpendicular MWCNTs. We further assumed that $w_\perp$ was directly proportional to $M_{n\,PTMSPMA}$ since $M_{n\,PTMSPMA}$ determines the number of chemical bonds between MWCNTs. Therefore, φ_p and $M_{n\,PTMSPMA}$ are the only two variables in eq 1 with an independent fitting parameter of proportionality factor between $M_{n\,PTMSPMA}$ and $w_\perp$. By varying the proportionality factor, $w_\perp = 3.98 \times 10^{-6}\, kTM_{n\,PTMSPMA}$ is found to be the best fit. The best fit theoretical plot in Figure 3 indicates an abrupt slope change around $M_{n\,PTMSPMA}$ of 11000. When $M_{n\,PTMSPMA}$ is below 11000, the percolation threshold decreases dramatically with the increase of $M_{n\,PTMSPMA}$, whereas, when $M_{n\,PTMSPMA}$ is above 11000, the increase of $M_{n\,PTMSPMA}$ only leads to a slight decrease of percolation threshold, which is in good agreement with the experimental results. $w_\perp = 3.98 \times 10^{-6}\, kTM_{n\,PTMSPMA}$ can be further applied to estimate interaction potentials between MWCNTs. For P3HT-*b*-PTMSPMA with $M_{n\,PTMSPMA}$ of 18300, $w_\perp$ was calculated to be $7.28 \times 10^{-2} kT$. Consequently, the interaction potential between two MWCNTs was estimated to be in the range of $7.28 \times 10^{-2} kT$ to $16.35kT$, corresponding to the situations that two MWCNTs are perpendicularly interacted and parallel interacted over their entire length, respectively. This is a reasonable estimation since previous research has proved that an interaction potential $\sim kT$ is sufficient to overcome the thermal energy of two colloidal objects and induce their flocculation.[48] All these results quantitatively support our proposed mechanism that the chemical bonding interactions introduced by the hydrolysis and the condensation of PTMSPMA block are the major driving force for the gelation of MWCNTs.

Characterization of MWCNT Aerogels. Chemical bonding interactions not only decrease the CGC of MWCNTs but also chemically cross-link and strengthen the MWCNT wet gel. Therefore, the chemically cross-linked CNT wet gel represents a more advantageous precursor of MWCNT aerogels than physically cross-linked CNT wet gel, which is mechanically weak, and some physical interactions may become invalid or diminished after the removal of the solvent. In our study, MWCNT wet gel can be freeze-dried to obtain MWCNT aerogels without collapse due to its robust institution. A systematical investigation of the MWCNT aerogel properties was performed on the aerogels derived from P3HT-*b*-PTMSPMA with $M_{n\,PTMSPMA}$ of 13000 (P3HT-*b*-$PTMSPMA_{13000}$) since such a polymer not only led to the lowest CGC but also favored the formation of ultralight MWCNT aerogels due to its relatively low molecular weight.

The bulk densities of the MWCNT aerogels fabricated from different P3HT-*b*-PTMSPMAs at the CGCs of MWCNTs are listed in Table 1. MWCNTs dispersed using P3HT-*b*-$PTMSPMA_{13000}$ resulted in the aerogel with a density of 4 mg/cm^3, which represents the lowest density ever for the free-standing monolithic CNT aerogels, and is only slightly larger than the lowest recorded aerogel density in the literature (3 mg/cm^3).[49] The picture of this ultralight MWCNT aerogel (MWCNT aerogel-13000/0.3, where 13000 and 0.3 denote the molecular weight of PTMSPMA and concentration of MWCNTs, respectively) in Figure 1 indicates a crack-free monolith. The overall shape of the aerogel, which is cylindrical in this case, was controlled by the mold used for gelation.

To optimize the mechanical properties of the ultralight MWCNT aerogels, its structure needs to be elaborately designed. Honeycomb structure is applied in honey bee nests for its excellent structural efficiency, that is, using less material to construct a given volume architecture with high strength to weight ratio. To achieve this efficient structure in the MWCNT aerogels, a modified ice-template approach was applied to the MWCNT wet gel.[50−52] The MWCNT wet gel was unidirectionally frozen by liquid nitrogen. Under such a condition, pseudo-steady-state continuous growth of ice crystals generated an array of micrometer-sized polygonal ice rods parallel with the freezing direction. The ice rods acted as the templates for the honeycomb structures and could be removed by freeze-drying to produce MWCNT aerogels with ordered honeycomb structures. The SEM image of MWCNT aerogel-13000/0.3 (Figure 4a) indicates macroporous honeycomb morphology with the honeycomb cell size in the range of 50−150 μm. The honeycomb wall composed of the tangled MWCNTs is less than 100 nm thick (Figure 4b), which is exceptionally thin compared to the honey-

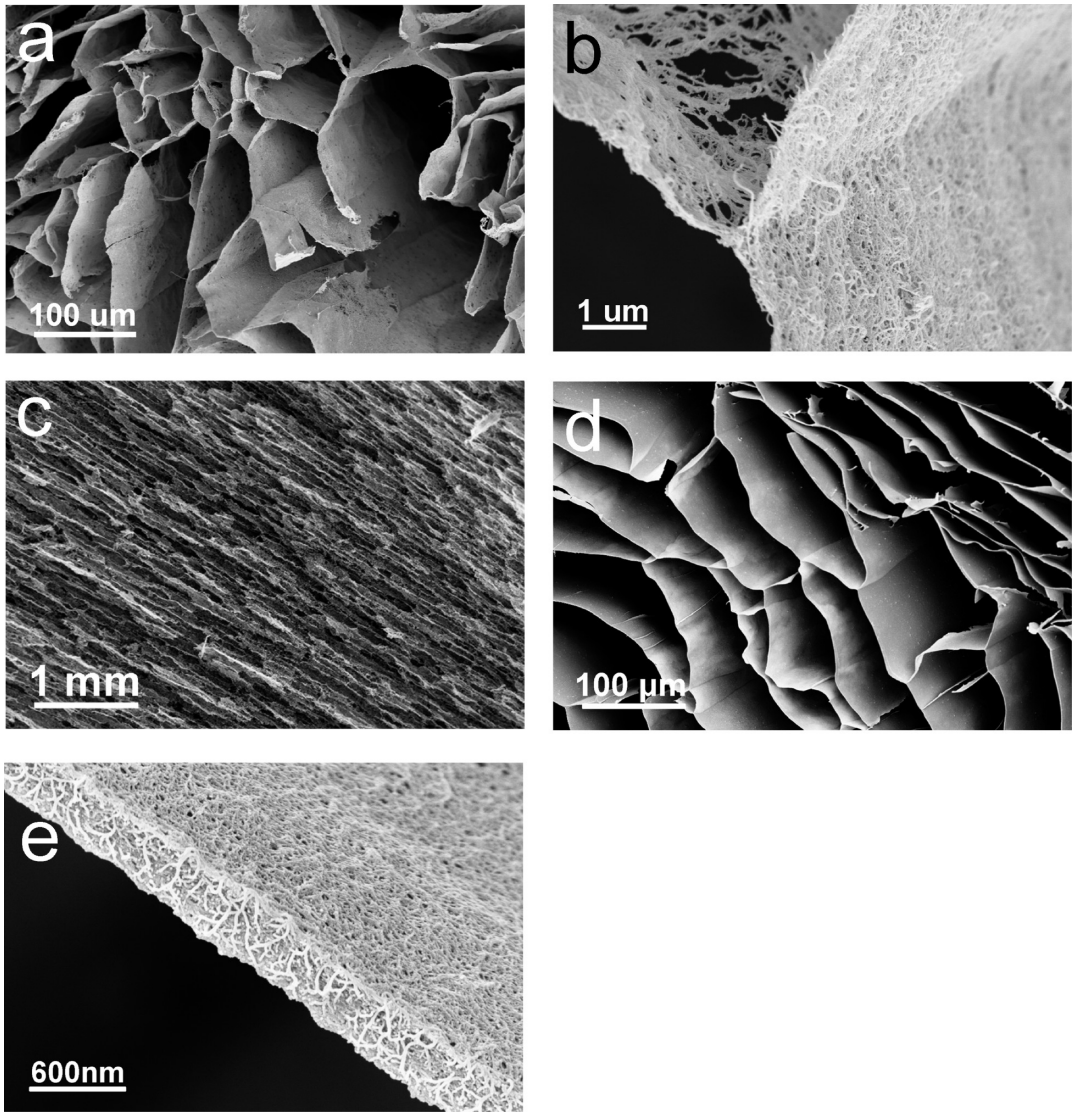

Figure 4. SEM images showing the morphology and structure of MWCNT aerogels. (a) Surface morphology of MWCNT aerogel-13000/0.3 indicating a honeycomb structure, (b) honeycomb wall of MWCNT aerogel-13000/0.3, (c) vertical section image of MWCNT aerogel-13000/0.3 indicating straight and parallel channels, (d) surface morphology of MWCNT aerogel-13000/1.0, (e) honeycomb wall of MWCNT aerogel-13000/1.0.

comb cell. Such a high cell to wall ratio, rarely reported for the honeycomb structure, indicates the ultralow density of the MWCNT aerogels. It is also worth noting that the honeycomb wall is not uniform and contains defects since the aerogel was built at the CGC of MWCNTs. The inner structure of the MWCNT aerogel-13000/0.3 was investigated by examining its vertical section. As shown in Figure 4c, straight and parallel channels were observed, indicating the anisotropic structure of the aerogels. To study the influence of MWCNT concentration on the honeycomb structures, MWCNT aerogels derived from 1.0 mg/mL MWCNTs dispersed by P3HT-*b*-PTMSPMA$_{13000}$ (MWCNT aerogel-13000/1.0) were investigated. As shown in Figure 4d, a more ordered and less defected honeycomb structure was observed with its honeycomb cell dimension comparable to that of MWCNT aerogel-13000/0.3, indicating that the cell dimension was mainly determined by the ice rod templates instead of the MWCNT concentration. However, MWCNT concentration had a remarkable influence on the honeycomb wall. As indicated in Figure 4e, the honeycomb wall of MWCNT aerogel-13000/1.0 is more uniform and thicker (~400 nm) than that of MWCNT aerogel-13000/0.3.

Besides the unique macroporous honeycomb structure, the MWCNT aerogels were found to have mesopores developed in the honeycomb walls, indicating that the aerogels are hierarchically porous materials. The mesoporosity of the MWCNT aerogel-13000/0.3 was quantitatively characterized by nitrogen adsorption/desorption experiments. The adsorption/desorption isomers shown in Figure 5a represented a IUPAC type IV curve, characteristic of mesoporous (2−50 nm pore diameter) materials.[53,54] The explicit adsorption/desorp-

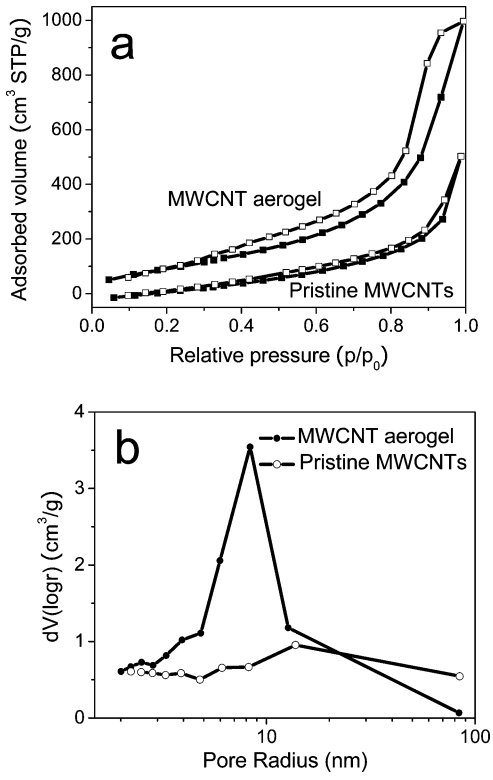

Figure 5. (a) N_2 adsorption (□) and desorption (■) isotherms of MWCNT aerogel and pristine MWCNTs. The isotherms of pristine MWCNTs are vertically shifted −100 cm^3 STP/g^{-1} for visual clarity. (b) BJH mesophore size distribution of MWCNT aerogel (●) and pristine MWCNTs (○).

tion hysteresis loop at the high relative pressure suggests that the MWCNT aerogels were highly mesoporous. By fitting the isotherms to the Brunauer−Emmett−Teller (BET) model, the surface area of the MWCNT aerogels was characterized to be 580 m^2/g. The mesopore size distribution which was calculated by the Barrett−Joyner−Halenda (BJH) method,[55] depicted a narrow peak centered at 8 nm (Figure 5b). The pristine MWCNTs were also investigated by a nitrogen adsorption/desorption experiment to compare with the aerogels. The isotherms shown in Figure 5a were essentially between IUPAC type II and IV. The adsorption isotherm of pristine MWCNTs resembled that of the MWCNT aerogels, signifying that the morphology and structure of MWCNTs in the aerogels were identical to those of pristine MWCNTs. This result suggests that both the structure and intrinsic properties of pristine MWCNTs remain intact during the aerogel fabrication process. The desorption isotherm of the pristine MWCNTs shows less hysteresis when compared to that of the MWCNT aerogels, indicating less porosity and different pore texture. The surface area of pristine MWCNTs was characterized to be 241 m^2/g, which is only 41.5% of that of the MWCNT aerogels. The surface area difference is caused by the different dispersion levels of MWCNTs in two systems. As-produced pristine MWCNTs form aggregates with partial surface area available for nitrogen adsorption, while MWCNTs exist as individual tubes in the aerogels, providing entire surface area. The better dispersion of MWCNTs in aerogels is also indicated by the mesopore size distribution where the mesopore size distribution of MWCNT aerogels is much narrower that that of as-produced pristine MWCNTs as indicated in Figure 5b.

Regardless of their ultralight density, the MWCNT aerogels are mechanically robust as indicated by the compression test. The MWCNT aerogel can be repeatedly compressed down to 5% of its original volume and recovers most of its volume after the release of compression (a video and images of the compressing and recovering process can be found in Supporting Information). Figure 6 panels a and b show the compressive stress (σ) and strain (ϵ) diagrams of the compression test with the stress loaded along (out-of-plane compression) and normal to (in-plane compression) the honeycomb cell axis direction, respectively. The hysteresis loop formed by the loading and unloading curves represents a typical stress−strain diagram of elastomeric open cell foams.[56] The compression loading curves indicate that the MWCNT aerogels can be compressed down to 5% of their original volume from both directions by low stress, indicating high porosity of the MWCNT aerogels. The unloading curves show that the stress remains above zero until the strain is zero, sug-

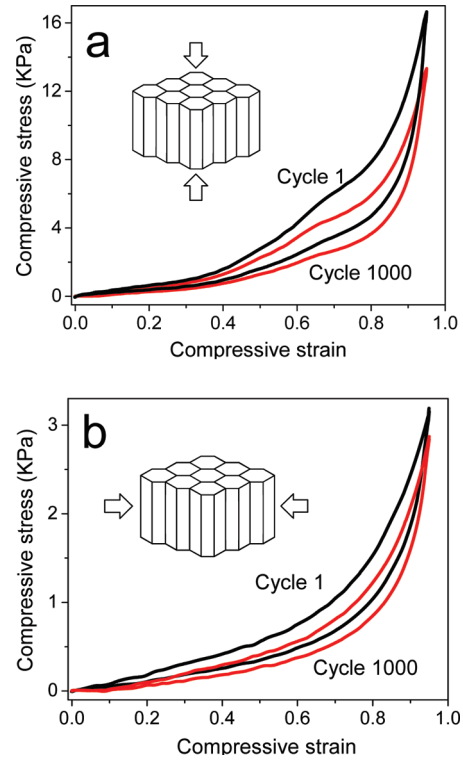

Figure 6. Compressive stress−strain diagrams of MWCNT aerogel-13000/0.3: (a) stress loaded along honeycomb cell axis; (b) stress loaded normal to honeycomb cell axis. The black and red curves represent the first and 1000th cycle during a fatigue cyclic compressive test.

gesting rapid and complete recovery of the highly compressed MWCNT aerogels. Despite their broadly similar shapes, the stress−strain diagrams of out-of-plane deformation and in-plane deformation are different in details due to the anisotropic structure of the MWCNT aerogels. First, the out-of-plane compression stress is much higher than the in-plane stress at the same strain (16.6 *vs* 3.1 KPa at ϵ of 0.95) because honeycombs are stronger and stiffer along the cell axis than normal to the cell axis.[57] Second, the out-of-plane compression diagram has three regimes. The linear-elastic regime at $\epsilon < 0.33$ records the elastic bending of cell walls. The nonlinear regime at $0.33 < \epsilon < 0.80$ has an increased slope, which may be due to the elastic buckling of the cell walls. The densification regime at $\epsilon > 0.80$, where stress rises steeply with compression, is because the cell walls begin to impinge upon each other. In contrast, the in-plane stress−strain diagram has two regions with a linear-elastic region at $\epsilon < 0.60$ followed by a densification region. This two-region diagram was also observed in foam-like CNT films.[58] In addition, the MWCNT aerogels were subjected to a fatigue cyclic compression test ($\epsilon = 0.95$) by undergoing 1000 loading/unloading cycles. The stress−strain diagram of cycle 1000 is identical to that of cycle 1 except that the compressive stress at ϵ of 0.95 decreases slightly to 87.1% and 90.2% of the original values for the out-of-plane and in-plane compression, respectively. Actually, the stress decreased gradually for the first 100 cycles and then leveled off in the subsequent cycles. The thickness reduction of the MWCNT aerogels after the fatigue test, which was obtained as the strain where the stress approaches zero at cycle 1000, is about 5% and 8% for the direction along and normal to the cell axis, respectively (Supporting Information, Figure S3). The fatigue test demonstrates the robust mechanical properties of the MWCNT aerogel attributed to both the outstanding mechanical properties of MWCNTs and the cross-linking between MWCNTs. When the compressing stress is applied to the aerogel, the MWCNTs tend to be bent instead of slipping past each other. Consequently, the strain energy is stored within the MWCNT aerogel, and recovery of the compressed aerogel to its original volume is driven by the release of the strain energy.

MWCNT-aerogel-13000/0.3 shows a conductivity of 3.2×10^{-2} S · cm^{-1}. Although the conductivity is significantly high for a material with a density of 4 mg/cm^3, it is still not as high as expected considering the conductivity of individual MWCNTs. We believe that the low conductivity of the MWCNT aerogels is due to the presence of the insulating PTMSPMA at the junction between MWCNTs since MWCNT-aerogel-18300/0.3, which has almost identical composition as MWCNT-aerogel-13000/0.3 except higher PTMSPMA content, shows a lower conductivity of 7.9×10^{-3} S · cm^{-1}. The conductivity of MWCNT-aerogel-9600/1.2 was characterized to have a higher conductivity of 0.26 S · cm^{-1} due to both the lower PTMSPMA content and higher MWCNT concentration. A high-current pulse method was applied to increase the conductivity of the aerogels.[24] By applying 15 ms 100 mA current pulses at an interval of 30 s, we observed stepwise increase of the conductivity, and after 20 pulses the conductivity reached a steady value of 0.67 S · cm^{-1} (Supporting Information, Figure S4), which is 20 times higher than the initial conductivity. The increase of the conductivity was irreversible indicating that the pulse may cause some permanent effect on the aerogels. The current pulses could initiate the decomposition of insulating polymers at the junction of MWCNTs. However, both SEM and mechanical studies on current-pulse-treated MWCNT aerogels indicated no property changes, suggesting that the high-current pulse did not cause the decomposition of polysilsesquioxane which cross-linked the MWCNT aerogels.

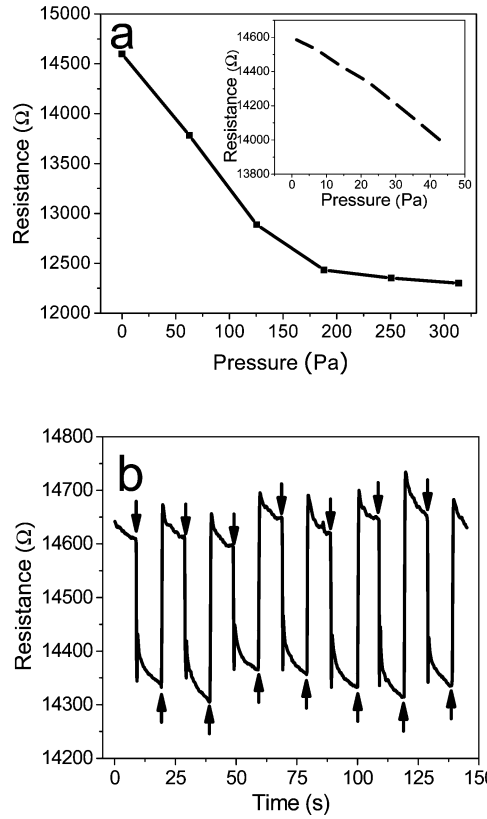

Figure 7. (a) The resistance change of MWCNT aerogel with applied pressure. At low pressure range, the resistance varies linearly with the pressure (inset). (b) Change of MWCNT aerogel resistance with loadings. Arrows indicate the moments of the application and release of loading.

MWCNT Aerogels for Pressure and Chemical Vapor Sensing. The compression recovery and conductive properties of the MWCNT aerogels lead to the pressure responsive property (*i.e.*, the resistance changes with the applied pressure). The correlation between the MWCNT aerogel resistance and the applied pressure along the honeycomb cell axis direction was investigated. As shown

in Figure 7a, the resistance of the MWCNT aerogels decreases linearly with the applied pressure from 0 to 180 Pa. A detail investigation in this pressure range indicates that even a pressure as low as 5 Pa can cause a remarkable change in the resistance (inset of Figure 7a), demonstrating the potential application of the MWCNT aerogel as an ultrasensitive pressure sensor. The response of aerogel resistance to the applied pressure becomes smaller when the pressure is higher than 180 Pa. We believe that such a resistance change profile is due to the pressure-induced increment of the MWCNT network density of the aerogels. Upon the application of the pressure, the aerogels are compressed and the MWCNT network is condensed, leading to the decrease of the resistance. The MWCNT network density in the uncompressed aerogels is equal to the percolation threshold at which the wet gel forms. A small pressure (0−180 Pa) increases the MWCNT network density around the percolation threshold, and greatly decreases the resistance of the aerogels. Such dramatic reduction of resistance is in good agreement with the percolation theory stating that a slight increase of the MWCNT concentration around the percolation threshold can noticeably increase conductivity. In contrast, applying a larger pressure (>180 Pa) onto the MWCNT aerogels generates a MWCNT network density well above the percolation threshold where the conductivity is not sensitive to the MWCNT network density increase according to the percolation theory, leading to a flat pressure *vs* resistance curve as shown in Figure 7a. The resistance change of the MWCNT aerogels in response to repeated loading and unloading of pressure (25 Pa) (Figure 7b) shows an instant resistance decrease (<0.2 S) with the loading of pressure, while, following the unloading of pressure, a complete and fast (<0.4 S) recovery was observed. The cycling measurement indicates that resistance change of the MWCNT aerogels with pressure is reproducible, which is due to the excellent compression recoverable capability of the MWCNT aerogels. Such intriguing pressure responsive properties of the MWCNT aerogel make it a promising candidate for pressure sensing.

The MWCNT aerogels have potential applications as sorption-based chemoresistance vapor sensors since their hierarchical porous structures not only provide high surface area but also facilitate the analyte diffusion in the aerogel.[59,60] The response of the MWCNT aerogels resistance to chloroform vapor was investigated (Supporting Information). As shown in Figure 8a, the resistance of the MWCNT aerogels increases to a saturated value in 0.5 s upon exposure to the vapor, and completely recovers in 0.5 s upon exposure to air even at very low vapor concentration. The detection limit was characterized to be 1 ppb. Alternating exposure of the MWCNT aerogels to chloroform vapor and air demonstrates reproducible response and recovery. As a control experiment, a MWCNT thin film (~1 μm), which has the same composition as the MWCNT aerogels, was prepared by casting the MWCNT/P3HT-*b*-PTMSPMA dispersion on a glass substrate. The sensory response of the MWCNT thin film as shown in Figure 8b demonstrates a significantly slower response (4−10 s) and much higher detection limit (37 ppb) compared to the MWCNT aerogels, indicating that the unique hierarchical porous structure improves the performance of the MWCNT aerogels as a chemoresistance vapor sensor.

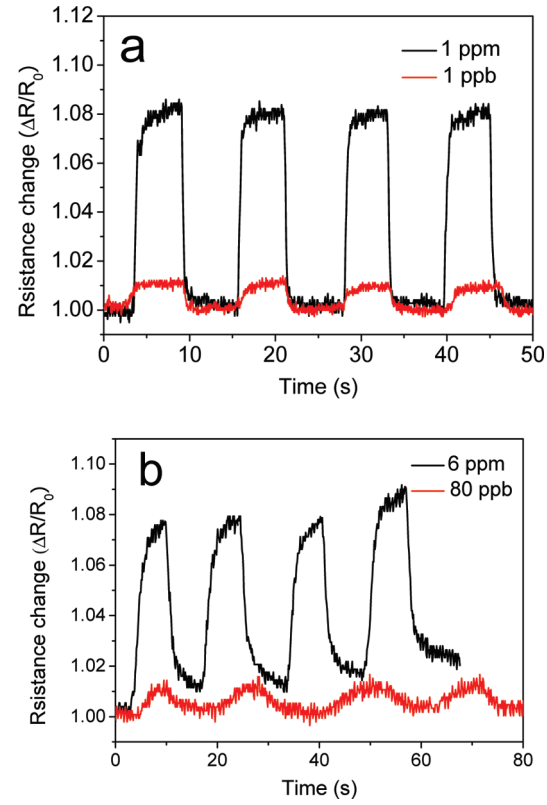

Figure 8. The resistance change of (a) MWCNT aerogel and (b) MWCNT thin film upon exposure to chloroform vapor. The bias voltage is fixed at 0.1 V.

CONCLUSION

We have fabricated the lightest free-standing monolithic MWCNT aerogels with a density of 4 mg/cm^3. The strong chemical bonding interactions between MWCNTs played a key role in the fabrication, which was proved both experimentally and theoretically. The MWCNT aerogel has an anisotropic macroporous honeycomb structure with straight and parallel honeycomb channels and mesoporous honeycomb walls. The MWCNT aerogel is a hierachically porous material with a surface area of 580 m^2/g and electrical conductivity of 3.2×10^{-2} S·cm^{-1} (0.67 S·cm^{-1} after high-current pulse treatment). The MWCNT aerogel demonstrates excellent compression recovery property. The unique anisotropic honeycomb structure combined with the hierarchical porosity with large surface area, compres-

sion recovery property, and high electrical conductivity makes the MWCNT aerogel promising for applications as chemoresistant vapor sensor and ultrasensitive pressure sensor. Other potential applications of the MWCNT aerogel may include catalyst supports and novel electrodes.

METHODS

Materials. P3HT-*b*-PTMSPMA was synthesized by reversible addition−fragmentation chain transfer (RAFT) polymerization of 3-(trimethoxysilyl) propyl methacrylate using P3HT trithiocarbonate compound[42] as the RAFT agent (Supporting Information, Scheme S1). Three P3HT-*b*-PTMSPMAs with different PTMSPMA molecular weight were synthesized using the same P3HT RAFT agent. Table 1 lists the number average molecular weight (M_n) of P3HT-*b*-PTMSPMAs and molecular weight of PTMSPMA block ($M_{n\,PTMSPMA}$), which was calculated by multiplying M_n with the weight percentage of PTMSPMA in P3HT-*b*-PTMSPMA determined by ^{1}H NMR spectrum (Supporting Information, Figure S5). MWCNTs were purchased from Nanolab (diameter of 10−20 nm, length of 5−20 μm, and purity beyond 95%) and were used as-received without further purification or chemical modification.

Characterization. Molecular weight of P3HT-*b*-PTMSPA was determined by size exclusion chromatography (SEC, A JASCO HPLC system equipped with PLgel 5 μm MIXED-C column) using polystyrene as standard. Morphology of the MWCNT aerogel was characterized by scanning electron microscope (SEM, ZEISS ULTRA55). The nitrogen adsorption/desorption experiment was carried out on Nova 4200e. Samples were dried at 130 °C for 4 h before the measurement. The compression tests were carried out on MTS Tytron 250 with loading capacity from 0.001 to 250 N at a constant loading and unloading speed of 0.05 mm/s. Cubic test pieces with a dimension of 1 cm × 1 cm × 1 cm were cut from the MWCNT aerogel. The conductivity of the MWCNT aerogel was measured by a typical four-probe conductivity measurement setup (Supporting Information, Figure S6) using a Keithley-2400 digital sourcemeter.

Acknowledgment. This work is supported by National Science Foundation (DMR 0746499). The authors are grateful to Dr. Quanfang Chen for the help in mechanical property studies.

Supporting Information Available: TEM image of dispersed MWCNTs, gelation time of MWCNT dispersion with different concentrations of P3HT-*b*-PTMSPMA and temperature, P3HT-*b*-PTMSPMA chain density on the MWCNT surface, video and images demonstrating compression recovery property of the MWCNT aerogel, determination of thickness reduction of MWCNT aerogel after fatigue test, conductivity evaluation with current pulse, synthetic scheme, and ^{1}H NMR spectrum of P3HT-*b*-PTMSPAM, the setup of the four-probe conductivity measurement, and chloroform vapor sensing studies. This material is available free of charge *via* the Internet at http://pubs.acs.org.

REFERENCES AND NOTES

1. Wu, Z.; Chen, Z.; Du, X.; Logan, J. M.; Sippel, J.; Nikolou, M.; Kamaras, K.; Reynolds, J. R.; Tanner, D. B.; Hebard, A. F. Transparent, Conductive Carbon Nanotube Films. *Science* **2004**, *305*, 1273–1276.
2. Zhang, M.; Fang, S.; Zakhidov, A. A.; Lee, S. B.; Aliev, A. E.; Williams, C. D.; Atkinson, K. R.; Baughman, R. H. Strong, Transparent, Multifunctional, Carbon Nanotube Sheets. *Science* **2005**, *309*, 1215–1219.
3. Mamedov, A. A.; Kotov, N. A.; Prato, M.; Guldi, D. M.; Wicksted, J. P; Hirsch, A. Molecular Design of Strong Single-Wall Carbon Nanotube/Polyelectrolyte Multilayer Composites. *Nat. Mater.* **2002**, *1*, 190–194.
4. Zhang, D.; Ryu, K.; Liu, X.; Polikarpov, E.; Ly, J.; Tompson, M. E.; Zhou, C. Transparent, Conductive, and Flexible Carbon Nanotube Films and Their Application in Organic Light-Emitting Diodes. *Nano Lett.* **2006**, *6*, 1880–1886.
5. Pasquier, A. D.; Unalan, H. E.; Kanwal, A.; Miler, S.; Chhowalla, M. Conducting and Transparent Single-Wall Carbon Nanotube Electrodes for Polymer−Fullerene Solar Cells. *Appl. Phys. Lett.* **2005**, *87*, 203511.
6. Zou, J.; Tran, B.; Huo, Q.; Zhai, L. Transparent Carbon Nanotube/Poly(3,4-ethylenedioxythiophene) Composite Electrical Conductors. *Soft Materials* **2009**, *7*, 355–365.
7. Koziol, K.; Vilatela, J.; Moisala, A.; Motta, M.; Cunniff, P.; Sennett, M.; Windle, A. High-Performance Carbon Nanotube Fiber. *Science* **2007**, *318*, 1892–1895.
8. Li, Y.-L.; Kinloch, L. A.; Windle, A. Direct Spinning of Carbon Nanotube Fibers from Chemical Vapor Deposition Synthesis. *Science* **2004**, *304*, 276–278.
9. Fan, S.; Chapline, M. G.; Franklin, N. R.; Tombler, T. W.; Cassell, A. M.; Dai, H. Self-Oriented Regular Arrays of Carbon Nanotubes and Their Field Emission Properties. *Science* **1999**, *283*, 512–514.
10. Pushparaj, V. L.; Shaijumon, M. M.; Kumar, A.; Murugesan, S.; Ci, L.; Vajtai, R.; Linhardt, R. J.; Nalamasu, O.; Ajayan, P. M. Flexible Energy Storage Devices Based on Nanocomposite Paper. *Proc. Natl. Acad. Sci. U.S.A.* **2007**, *104*, 13574–13577.
11. Lee, S. W.; Kim, B. -S.; Chen, S.; Shao-Horn, Y.; Hammond, P. T. Layer-by-Layer Assembly of All Carbon Nanotube Ultrathin Films for Electrochemical Applications. *J. Am. Chem. Soc.* **2009**, *131*, 671–679.
12. Li, H. J.; Lu, W. G.; Li, J. J.; Bai, X. D.; Gu, C. Z. Multichannel Ballistic Transport in Multiwall Carbon Nanotubes. *Phys. Rev. Lett.* **2005**, *95*, 086601.
13. Yao, Z.; Kane, C. L.; Dekker, C. High-Field Electrical Transport in Single-Wall Carbon Nanotubes. *Phys. Rev. Lett.* **2000**, *84*, 2941–2944.
14. Wong, E. W.; Sheehan, P. E.; Lieber, C. M. Nanobeam Mechanics: Elasticity, Strength, and Toughness of Nanorods and Nanotubes. *Science* **1997**, *277*, 1971–1975.
15. Yu, M.-F.; Lourie, O.; Dyer, M. J.; Moloni, K.; Kelly, T. F.; Ruoff, R. S. Strength and Breaking Mechanism of Multiwalled Carbon Nanotubes Under Tensile Load. *Science* **2000**, *287*, 637–640.
16. Pang, L. S. K.; Saxby, J. D.; Chatfield, S. P. Thermogravimetric Analysis of Carbon Nanotubes and Nanoparticles. *J. Phys. Chem.* **1993**, *97*, 6941–6942.
17. Masarapu, C.; Ok, J. T.; Wei, B. Thermal Stability of Carbon-Nanotube-Based Field Emission Diodes. *J. Phys. Chem. C* **2007**, *111*, 12112–12115.
18. Pierre, A. C.; Pajonk, G. M. Chemistry of Aerogels and Their Applications. *Chem. Rev.* **2002**, *102*, 4243–4266.
19. Hüsing, N.; Schubert, U. Aerogels—Airy Materials: Chemistry, Structure, and Properties. *Angew. Chem., Int. Ed.* **1998**, *37*, 22–45.
20. Yoldas, B. E.; Annen, M. J.; Bostaph, J. Chemical Engineering of Aerogel Morphology Formed under Nonsupercritical Conditions for Thermal Insulation. *Chem. Mater.* **2000**, *12*, 2475–2484.
21. Conroy, J. F. T.; Hosticka, B.; Davis, S. C.; Smith, A. N.; Norris, P. M. Microscale Thermal Relaxation During Acoustic Propagation in Aerogel and Other Porous Media. *Microscale Thermophys. Eng.* **1999**, *3*, 199–215.
22. Saquing, C. D.; Kang, D.; Aindow, M.; Erkey, C. Investigation of the Supercritical Deposition of Platinum Nanoparticles into Carbon Aerogels. *Microporous Mesoporous Mater.* **2005**, *80*, 11–23.
23. Li, J.; Wang, X.; Huang, Q.; Gamboa, S.; Sebatian, P. J. Studies on Preparation and Performances of Carbon Aerogel Electrodes for the Application of Supercapacitor. *J. Power Sources* **2006**, *158*, 784–788.
24. Bryning, M. B.; Milkie, D. E.; Islam, M. F.; Hough, L. A.; Kikkawa, J. M.; Yodh, A. G. Carbon Nanotube Aerogels. *Adv. Mater.* **2007**, *19*, 661–664.

25. Gui, X.; We, J.; Wang, K.; Cao, A.; Zhu, H.; Jia, Y.; Shu, Q.; Wu, D. Carbon Nanotube Sponges. *Adv. Mater.* **2010**, *22*, 617–621.
26. Bug, A. L. R.; Safran, S. A.; Grest, G. S; Webman, I. Do Interactions Raise or Lower a Percolation Threshold. *Phys. Rev. Lett.* **1985**, *55*, 1896–1899.
27. Safran, S. A.; Webman, I.; Grest, G. S. Percolation in Interacting Colloids. *Phys. Rev. A* **1985**, *32*, 506–511.
28. Poon, W. C. K.; Haw, M. D. Mesoscopic Structure Formation in Colloidal Aggregation and Gelation. *Adv. Colloid Interface Sci.* **1997**, *73*, 71–126.
29. Te Nijenhuis, K. *Thermoreversible Network: Viscoelastic Properties and Structure of Gels*; Springer: Berlin, 1997.
30. Zou, J.; Liu, L.; Chen, H.; Khondaker, S. I.; Huo, Q.; McCullough, R. D.; Zhai, L. Dispersion of Pristine Carbon Nanotubes Using Conjugated Block Copolymers. *Adv. Mater.* **2008**, *20*, 2055–2060.
31. Zou, J.; Chen, H.; Chunder, A.; Yu, Y.; Huo, Q.; Zhai, L. A Simple Preparation of Superhydrophobic and Conductive Nanocomposite Coating from a Carbon Nanotube-Conjugated Block Copolymer Dispersion. *Adv. Mater.* **2008**, *20*, 3337–3341.
32. Zou, J.; Khondaker, S. I.; Huo, Q.; Zhai, L. A General Strategy to Disperse and Functionalize Carbon Nanotubes Using Conjugated Block Copolymers. *Adv. Funct. Mater.* **2009**, *19*, 479–483.
33. Zou, P.; Shi, G. -Y.; Pan, C. -Y. Large-Compound Vesicle-Encapsulated Multiwalled Carbon Nanotubes: A Unique Route to Nanotube Composites. *J. Polym. Sci., Part A: Polym. Chem.* **2009**, *47*, 3669–3679.
34. Xiao, Q.; He, S.; Liu, L.; Guo, X.; Shi, K.; Du, Z.; Zhang, B. Coating of Multiwalled Carbon Nanotubes with Crosslinked Silicon-Containing Polymer. *Compos. Sci. Technol.* **2008**, *68*, 321–328.
35. Hough, L. A.; Islam, M. F.; Hammouda, B.; Yodh, A. G.; Heiney, P. A. Structure of Semidilute Single-Wall Carbon Nanotube Suspensions and Gels. *Nano Lett.* **2006**, *6*, 313–317.
36. Chen, J.; Xue, C.; Ramasubramaniam, R.; Liu, H. A New Method for the Preparation of Stable Carbon Nanotube Organogels. *Carbon* **2006**, *44*, 2142–2146.
37. Fukushima, T.; Kosaka, A.; Ishimura, Y.; Yamamoto, T.; Takigawa, T.; Ishii, N.; Aida, T. Molecular Ordering of Organic Molten Salts Triggered by Single-Walled Carbon Nanotubes. *Science* **2003**, *300*, 2072–2074.
38. Kovtyukhova, N. I.; Mallouk, T. E.; Pan, L.; Dickey, E. C. Individual Single-Walled Nanotubes and Hydrogels Made by Oxidative Exfoliation of Carbon Nanotube Ropes. *J. Am. Chem. Soc.* **2003**, *125*, 9761–9769.
39. Tung, Y. -C.; Chen, W. -C. Poly[2,7-(9,9-dihexylfluorene)]-*block*-poly[3-(trimethoxysilyl)propyl methacrylate] (PF-*b*-PTMSPMA) Rod−Coil Block Copolymers: Synthesis, Morphology and Photophysical Properties in Mixed Solvents. *React. Funct. Polym.* **2009**, *69*, 507–518.
40. Abdallah, D. J.; Weiss, R. G. Organogels and Low Molecular Mass Organic Gelators. *Adv. Mater.* **2000**, *12*, 1237–1247.
41. Vigolo, B.; Coulon, C.; Maugey, M.; Zakri, C.; Poulin, P. An Experimental Approach to the Percolation of Sticky Nanotubes. *Science* **2005**, *309*, 920–923.
42. Chiew, Y. C.; Glandt, E. D. Percolation Behaviour of Permeable and of Adhesive Spheres. *J. Phys. A* **1983**, *16*, 2599–2608.
43. Coniglio, A.; De Angelis, U.; Forlani, A. Pair Connectedness and Cluster Size. *J. Phys. A* **1977**, *10*, 1123–1139.
44. Hill, T. L. Molecular Clusters in Imperfect Gases. *J. Chem. Phys.* **1955**, *23*, 617–622.
45. Liu, C.; Zhang, J.; He, J.; Hu, G. Gelation in Carbon Nanotube/Polymer Composites. *Polymer* **2003**, *44*, 7529–7532.
46. Lu, Q.; Keskar, G.; Ciocan, R.; Rao, R.; Mathur, R. B.; Rao, A. M.; Larcom, L. L. Determination of Carbon Nanotube Density by Gradient Sedimentation. *J. Phys. Chem. B* **2006**, *110*, 24371–24376.
47. The average length and diameter of MWCNTs were obtained by statistical analysis of 100 MWCNTs in TEM images. The average length was lower than the length claimed by the manufacturer. The average diameter was in agreement with the claimed value when considering that the MWCNT surface was covered by a thin layer of P3HT-*b*-PTMSPMA.
48. Bonard, J.-M.; Stora, T.; Salvetat, J.-P.; Maier, F.; Stöckli, T.; Duschl, C.; Forró, L.; de Heer, W. A.; Châtelain, A. Purification and Size-Selection of Carbon Nanotubes. *Adv. Mater.* **1997**, *9*, 827–831.
49. Tillotson, T. M.; Hrubesh, L. W. Transparent Ultralow-Density Silica Aerogels Prepared by a Two-Step Sol−Gel Process. *J. Non-Cryst. Solids.* **1992**, *145*, 44–50.
50. Mukai, S. R.; Nishihara, H.; Tamon, H. Formation of Monolithic Silica Gel Microhoneycombs (SMHs) Using Pseudo-steady-state Growth of Microstructural Ice Crystals. *Chem. Commun.* **2004**, *7*, 874–875.
51. Nishihara, H.; Mukai, S. R.; Tamon, H. Preparation of Resorcinol−Formaldehyde Carbon Cryogel Microhoneycombs. *Carbon* **2004**, *42*, 899–901.
52. Nishihara, H.; Mukai, S. R.; Yamashita, D.; Tamon, H. Ordered Macroporous Silica by Ice Templating. *Chem. Mater.* **2005**, *17*, 683–689.
53. Gregg, S. J.; Sing, K. S. W. *Adsorption, Surface Area and Porosity*, 2nd ed.; Academic: New York, 1982.
54. Webb, P. A.; Orr, C. *Analytical Methods in Fine Particle Technology*; Micromeritics Instrument Corp.: Norcross, GA, 1997.
55. Barrett, E. P.; Joyner, L. G.; Halenda, P. P. The Determination of Pore Volume and Area Distributions in Porous Substances. I. Computations from Nitrogen Isotherms. *J. Am. Chem. Soc.* **1951**, *73*, 373–380.
56. Yu, W.; Li, Y.; Zheng, Y. P.; Lim, N. Y.; Lu, M. H.; Fan, J. Softness Measurement for Open-Cell Foam Materials and Human Soft Tissue. *Meas. Sci. Technol.* **2006**, *17*, 1785–1791.
57. Gibson, L. J.; Ashby, M. F. *Cellular Solids, Structure and Properties*, 2nd ed.; Pergamon: New York, 1997.
58. Cao, A.; Dickrell, P. L.; Sawyer, W. G.; Ghasemi-Nejhad, M. M.; Ajayan, P. M. Super-Compressible Foamlike Carbon Nanotube Films. *Science* **2005**, *25*, 1307–1310.
59. Sizgek, G. D.; Sizgek, E.; Griffith, C. S.; Luca, V. Mesoporous Zirconium Titanium Oxides. Part 2: Synthesis, Porosity, and Adsorption Properties of Beads. *Langmuir* **2008**, *24*, 12323–12330.
60. Sizgek, G. D.; Griffith, C. S.; Sizgek, E.; Luca, V. Mesoporous Zirconium Titanium Oxides. Part 3: Synthesis, Porosity, and Adsorption Properties of Unfunctionalized and Phosphonate-Functionalized Hierarchical Polycarylonitrile-F-127-Templated Beads. *Langmuir* **2009**, *25*, 11874–11882.
61. Iovu, M. C.; Craley, C. R.; Jeffries-EL, M.; Krankowski, A. B.; Zhang, R.; Kowalewski, T.; McCullough, R. D. Conducting Regioregular Polythiophene Block Copolymer Nanofibrils Synthesized by Reversible Addition Fragmentation Chain Transfer Polymerization (RAFT) and Nitroxide Mediated Polymerization (NMP). *Macromolecules* **2007**, *40*, 4733–4735.